ORCHIDEE-MICT-BIOENERGY: an attempt to represent the production of lignocellulosic crops for bioenergy in a global vegetation model

Wei Li[1], Chao Yue[1], Philippe Ciais[1], Jinfeng Chang[1], Daniel Goll[1], Dan Zhu[1], Shushi Peng[2], Albert Jornet-Puig[1]

[1]Laboratoire des Sciences du Climat et de l'Environnement, LSCE/IPSL, CEA-CNRS-UVSQ, Université Paris-Saclay, 91191 Gif-sur-Yvette, France
[2]Sino-French Institute for Earth System Science, College of Urban and Environmental Sciences, Peking University, Beijing 100871, China

Correspondence to: Wei Li (wei.li@lsce.ipsl.fr)

10

Abstract. Bioenergy crop cultivation for lignocellulosic biomass is increasingly important for future climate mitigation, and it is assumed on large scales in Integrated Assessment Models (IAMs) that develop future land use change scenarios consistent with the dual constraint of sufficient food production and deep de-carbonization for low climate warming targets. In most global vegetation models, there is no specific representation of crops producing lignocellulosic biomass, resulting in simulation biases of biomass yields and other carbon outputs, and in turn of future bioenergy production. Here, we introduced four new plant functional types (PFTs) to represent four major lignocellulosic bioenergy crops, eucalypt, poplar and willow, *Miscanthu*s, and switchgrass, in the global process-based vegetation model, ORCHIDEE. New parameterizations of photosynthesis, carbon allocation and phenology are proposed based on a compilation of field measurements. A specific harvest module is further added to the model to simulate the rotation of bioenergy tree PFTs based on their age dynamics. The resulting ORCHIDEE-MICT-BIOENERGY model is applied at 296 locations where field measurements of harvested biomass are available for different bioenergy crops. The new model can generally reproduce the global bioenergy crop yield observations. Biases of the model results related to grid-based simulations versus the point-scale measurements and the lack of fertilization and fertilization management practices in the model are discussed. This study sheds light on the importance of properly representing bioenergy crops for simulating their yields. The parameterizations of bioenergy crops presented here are generic enough to be applicable in other global vegetation models.

Geoscientific
Model Development
Discussions

1 Introduction

Biomass-derived fuels serve as an alternative energy source to substitute fossil fuel and are used by many countries to meet renewable energy and climate target (Karp and Shield, 2008; Meier et al., 2015; Robertson et al., 2017). Expanding bioenergy crop plantation is considered in future scenarios for energy security and climate change mitigation (Karp and

5   Shield, 2008; Robertson et al., 2017; Smith et al., 2016). For bioenergy production to provide economic and climate benefits, cultivated plants must have a high productivity and a high yield of harvestable biomass (Karp and Shield, 2008; Robertson et al., 2017; Whitaker et al., 2010). The first generation of bioenergy crops usually refers to grain and high-sugar crops like maize and sugarcane (Karp and Shield, 2008). These crops have high nutrient requirements which demand fertilizer additions causing high N_2O emissions to the atmosphere to achieve a high productivity (Melillo et al., 2009; Searchinger et

10   al., 2008). These grain and high-sugar crops are unlikely to be planted in large-scale for the purpose of bioenergy production because of the food demand pressure for fertile land and fertilizer (Alexandratos and Bruinsma, 2012; Gerland et al., 2014; United Nations, 2017). Compared to the first generation, the second generation bioenergy crops, known as lignocellulosic energy crops like giant miscanthus, swithgrass and short-rotation trees, are adapted to a wider range of climatic and soil conditions and require less nitrogen fertilizer (Cadoux et al., 2012; Miguez et al., 2008). Those second generation bioenergy

15   crops have potentials to be deployed on marginal lands to avoid direct and indirect land use change (LUC) carbon emissions and damage of ecosystem services (Robertson et al., 2017). They also appear to have less greenhouse gas (GHG) emissions and higher energy efficiency than the first generation bioenergy crops (Whitaker et al., 2010).

Bioenergy with carbon capture and storage (BECCS) is the main class of future negative emission technologies expected to result in net removal of atmospheric CO_2 (Smith et al., 2016). BECCS has been extensively assumed in Integrated

20   Assessment Models (IAMs) to develop land-based mitigation scenarios for low warming levels (Fuss et al., 2014; Popp et al., 2014). In most IAMs like IMAGE (Bouwman et al., 2006; Stehfest et al., 2014) and MAgPIE (Klein et al., 2014; Popp et al., 2011), second generation bioenergy crops are used as primary energy carriers (Popp et al., 2014). One output from IAMs is future land use maps based on different environmental, socioeconomic and policy constraints. These land use maps, after being translated into plant functional type (PFT) maps, can be used in grid-based dynamic global vegetation models

25   (DGVMs) to simulate the terrestrial carbon dynamics, biogeochemical (e.g. LUC carbon emissions) and biophysical (e.g. albedo and transpiration changes) effects of land use processes (Brovkin et al., 2013; Wilkenskjeld et al., 2014). Global vegetation models can provide in return to IAMs some valuable information like spatially explicit biomass density, crop yield and water availability (Bonsch et al., 2015, 2016; Stehfest et al., 2014). For example, dedicated bioenergy crop modelling has been implemented in a global vegetation model (LPJml) (Beringer et al., 2011; Heck et al., 2016), to simulate

30   biophysical yields and water availability as input data for MAgPIE (Bonsch et al., 2016).

In most global grid-based vegetation models, there is no dedicated PFTs to represent second-generation bioenergy crops. Instead, these plants are often represented by a generic crop PFT. Biases in simulated biomass production and resulting

carbon and energy balance thus arise when ignoring differences in carbon assimilation and phenology between generic crops and lignocellulosic bioenergy crops. Moreover, lignocellulosic woody bioenergy crops like eucalypt, poplar and willow cannot be properly represented by an herbaceous crop PFT. For example, eucalypt has a high maximum rate of carboxylation (V_{cmax}) but relatively low leaf area index (LAI) (Stape et al., 2004; Whitehead and Beadle, 2004). *Miscanthus* on the contrary,

5   has a relatively lower V_{cmax} (Wang et al., 2012; Yan et al., 2015) but a higher LAI (Heaton et al., 2008; Zub and Brancourt-Hulmel, 2010) than eucalypt (Whitehead and Beadle, 2004). Even if both *Miscanthus* and switchgrass are C4 crops, *Miscanthus* can achieve a significantly higher yield than switchgrass because of a higher efficiency of converting intercepted radiation into aboveground biomass than switchgrass (Heaton et al., 2008). The water, nitrogen and light use efficiencies are also higher for *Miscanthus* than for switchgrass, resulting in a higher rate of leaf photosynthesis in the former (Dohleman et

10   al., 2009). All these important differences between lignocellulosic bioenergy crops need to be considered, which calls for having a dedicated new model PFT for each species.

Similarly, the way that harvest is implemented for generic crops in global models (usually removing a fixed fraction of biomass, typically on the order of 50%) cannot be used for bioenergy crops. The harvest index (*HI*, harvested biomass as a fraction of aboveground biomass) is very different for grain crops and herbaceous bioenergy crops. In addition, most

15   vegetation models currently do not account for realistic rotations of ligneous bioenergy plants (e.g. poplar and eucalypt). Modeling the harvest of woody bioenergy crops should be based on rotation practices of typically a few years rather than on assuming annual full harvest like for herbaceous crops. This requires simulating forest age dynamics (Yue et al., 2017) to accurately represent the ligneous biomass harvest.

In this study, we aim to model biomass yields of four major lignocellulosic bioenergy crops in the global dynamic vegetation

20   model ORCHIDEE. We introduce the new bioenergy crop PFTs, adjust the parameters relevant to physiology, phenology and harvest process of bioenergy crops based on observations, and evaluate the simulated biomass yields using a new global dataset of field measurements.

2 Model development and parameterization

2.1 Model description

25   The proposed parameterizations of lignocellulosic bioenergy crops are based on an extended version of ORHCIDEE (Krinner et al., 2005) — ORCHIDEE-MICT (Guimberteau et al., 2017) which contains relevant features of gross land use change, wood harvest and forest age classes dynamics (Yue et al., 2017). The model simulates energy exchange, water balance and vegetation carbon processes in the ecosystem and is the land surface component of the French Earth System Model (ESM) IPSL-CM (Krinner et al., 2005). The principal processes related to carbon cycling comprise photosynthesis,

30   vegetation carbon allocation, autotrophic and heterotrophic respiration, plant phenology (e.g. leaf onset and senescence) and

litter and soil carbon dynamics (Krinner et al., 2005). ORCHIDEE-MICT further includes high-latitude related processes with new parameterizations of soil carbon vertical discretization, snow processes, and the SPITFIRE fire module (Guimberteau et al., 2017). Importantly, the representation of forest age dynamics in this version (Yue et al., 2017) allows us to simulate wood harvest based on rotation length practices, a prerequisite for simulating the woody yields.

5　Originally, there are 13 plant functional types (PFTs) in ORCHIDEE (Table 1) (Krinner et al., 2005). In order to represent the bioenergy crops, we introduced four new PFTs (Table 1). PFT14 is a tropical tree, representing eucalypt (*Eucalyptus spp.*); PFT15 is a temperate tree representing poplar (*Populus spp.*) and willow (*Salix spp.*); PFT16 and PFT17 are treated as crops, representing *Miscanthus* and switchgrass (*Panicum spp.*) respectively. The reason for separating *Miscanthus* and switchgrass into two PFTs is that they are significantly different in biomass yields and resource use efficiency (Dohleman et

10　al., 2009; Heaton et al., 2008). The default model equations of the four new bioenergy crop PFTs follow the ones of similar PFTs already defined in the model (Table 1), i.e. tropical broad-leaved evergreen (PFT2) for PFT14, temperate broad-leaved summer-green (PFT6) for PFT15, and C4 crop (PFT13) for PFT16 and PFT17. Some parameters were however adjusted specifically for their corresponding bioenergy crops based on field experiment or measurement data in **Section 2.3**.

2.2 Bioenergy biomass harvest module

15　The new module represents the periodical harvest of bioenergy crops, consisting of two sub-routines differentiating woody and herbaceous crops. For woody types, harvest is based on simulated forest age classes (see details in Yue et al., 2017). Briefly, each woody PFT is sub-divided into six cohort functional types (CFTs) corresponding to different age classes. The boundary of age classes is set as being PFT specific and defined based on maximum woody biomass (total of the sapwood and heartwood biomass). When the biomass of a young woody CFT reaches the upper boundary defining its age class, it is

20　moved to the next older CFT, and sequentially until it reaches the oldest CFT (mature). The fractional harvested area of a woody crop PFT in each grid cell is externally prescribed. Then, the harvest algorithm starts from the second youngest CFT, continues with the next older CFT, and eventually reverts to the youngest CFT until the prescribed harvested area is met. For woody bioenergy crops, we adjusted the fraction of aboveground biomass that is harvested (the harvest index denoted *HI*) and put harvested biomass into a separate bioenergy harvest pool rather than mixing it with the modeled wood product pools

25　existing for forest management harvest (Yue et al., 2017) or with an agricultural product pool for the two crop PFTs (PFT13 and 14, Table 1) as defined by Piao et al., (2009). The non-harvested biomass goes to litter. For herbaceous types, only the *HI* fraction of aboveground biomass is harvested (**Section 2.3.4**) after leaf senescence either at the end of growing season or if climate conditions like drought and low temperature trigger canopy senescence in the model. The remaining part of above- and belowground biomass goes to litter pools. Carbon in the bioenergy harvest pool is released to the atmosphere directly.

30　**2.3 Parameterization of bioenergy crops**

Most parameters in ORCHIDEE are PFT specific (Krinner et al., 2005). Since we aim to improve the biomass production performance of the four bioenergy crop PFTs, we adjusted parameters controlling carbon assimilation (**Section 2.3.1**), allocation (**Section 2.3.2**), phenology (**Section 2.3.3**) and harvest processes (**Section 2.3.4**) based on observed values at ecosystem or leaf scale (Table 2).

5   **2.3.1 Photosynthesis parameters**

The photosynthesis process at leaf level for C3 and C4 plants in ORCHIDEE-MICT is based on the extended version (Yin and Struik, 2009) of the Farquhar, von Caemmerer and Berry model (FvCB model) (Farquhar et al., 1980). The related parameters generally follow Yin and Struik (2009) except for the maximum rate of Rubisco activity (V_{cmax}) and maximum rate of electron transport under saturated light (J_{max}). The setting of V_{cmax} and J_{max} for C3 plants is based on Medlyn et al.

10   (2002) and Kattge and Knorr (2007) in order to account for the acclimation of V_{cmax} and J_{max} to temperature. In ORCHIDEE, V_{cmax25} (V_{cmax} at 25 ℃) is prescribed for each PFT, and J_{max} is calculated from the ratio (r_{JV}) between J_{max} and V_{cmax}:

$$J_{max} = V_{cmax} \times r_{JV} \tag{1}$$

r_{JV} is a function of growth temperature (T_{growth}) (Kattge and Knorr, 2007):

$$r_{JV} = a_{rJV} + b_{rJV} \times T_{growth} \tag{2}$$

15   where a_{rJV} and b_{rJV} is the acclimation parameters derived by fitting data from 36 plant species (Kattge and Knorr, 2007). For C4 plants, no acclimation is considered for V_{cmax} and J_{max}, and thus $b_{rJV} = 0$ and a_{rJV} is a fixed value (Table 2).

Because values of V_{cmax} and J_{max} are critical for determining carbon assimilation by bioenergy PFTs, we searched for published experimental data of these parameters for eucalypt, poplar, willow, *Miscanthus* and switchgrass and found 26 observation-based publications with 127 entries for V_{cmax} and 69 entries for J_{max} (Table S1).

20   Some observations of V_{cmax} and J_{max} were derived at other temperatures (Table S1) than 25 ℃, and we thus normalized these two temperature dependent variables to V_{cmax25}, J_{max25} (J_{max} at 25 ℃) using a modified Arrhenius function from Medlyn et al. (2002) and parameters for C3 and C4 plants from Yin and Struik (2009). The ranges of V_{cmax25}, J_{max25} and r_{JV25} (r_{JV} at 25 ℃, only for the studies reporting both V_{cmax} and J_{max}) are shown in Fig. 1a-c. V_{cmax25} values generally decrease from eucalypt > poplar and willow > *Miscanthus* ≥ switchgrass. The interquartile range of V_{cmax25} is large for eucalypt (N = 42) from 75 to

25   126 μmol m^{-2} s^{-1} and for poplar and willow (N = 30) from 57 to 165 μmol CO_2 m^{-2} s^{-1}. *Miscanthus* and switchgrass have a relatively smaller interquartile range of V_{cmax25} (17 to 32, N = 38 and 12 to 26, N = 17, respectively). We adjusted the prescribed parameters V_{cmax25} and a_{rJV} (Table 2) for each bioenergy crop PFT using a value close to the median value in the observation dataset (Fig. 1a,c, within a range of 10% of the median values). We also verified that J_{max25} from Equation (1) is also in the range of independent J_{max25} observations (Fig. 1b). Importantly, the observation-based estimates of V_{cmax25} and

J_{max25} for *Miscanthus* are significantly larger than for switchgrass (p = 0.02 and 0.09 respectively, Fig. 1a,b). Note that the ranges shown in Fig. 1 could be influenced by the sample size and number of studies.

We also adjusted other parameters including θ (the convexity factor of the response of rate of electron transport to irradiance), and $\alpha_{(LL)}$ (conversion efficiency of absorbed light into e- transport rate at strictly limiting light) and g_0 (residual

5   stomatal conductance when irradiance approaches zero) in the leaf-level photosynthesis equations of ORCHIDEE to match higher productivity based on field measurements or empirical data (Table 2). The detailed effects of these parameters on photosynthesis in the FvCB model can be found in Yin and Struik (2009). In brief, θ and $\alpha_{(LL)}$ are used in the calculation of J (photosynthesis rate limited by electron transport):

$$J = \frac{\alpha_{(LL)}I + J_{max} - \sqrt{(\alpha_{(LL)}I + J_{max})^2 - 4\theta J_{max}\alpha_{(LL)}I}}{2\theta}$$ (3)

10   Where I is the photon flux density absorbed by leaf photosynthetic pigments. g_0 is an intercept related to the estimation of g_s (stomatal conductance):

$$g_s = g_0 + \frac{A + R_d}{C_i - C_{i*}} f_{VPD}$$ (4)

Where A is the net photosynthesis rate, R_d is the day respiration, and C_i and C_{i*} are the intercellular CO_2 partial pressure and C_i-based CO_2 compensation point in the absence of R_d, respectively. f_{VPD} is factor of the effect of leaf-to-air vapor pressure

15   difference (Yin and Struik, 2009).

Specifically for bioenergy crop PFTs, we increased θ to 0.8 for PFT14 (eucalypt) based on Yin and Struik (2017) and to 0.84 for PFT16 (Miscanthus) based on field measurements from Dohleman and Long (2009). Light use efficiency and productivity are high for bioenergy crops (e.g. see reviews by Forrester, 2013; Heilman et al., 1996; Karp and Shield, 2008; Laurent et al., 2015; Lewandowski et al., 2003; McCalmont et al., 2017; Whitehead and Beadle, 2004; Zub and Brancourt-

20   Hulmel, 2010), and we thus set $\alpha_{(LL)}$ and g_0 to the maximum boundary in their ranges from Yin and Struik (2009) to favors high light use efficiency and productivity characteristic of bioenergy cultivars (Table 2).

Morphological plant traits are also of key importance to the canopy-level productivity (Chang et al., 2015). The specific leaf area (*SLA*) in ORCHIDEE is a PFT-specific constant (Krinner et al., 2005). *SLA* for different bioenergy crops from our data compilation (164 entries in Table S1) is shown in Fig. 1d. A factor of 2 is used to convert the *SLA* unit from $m^2\ g^{-1}$ dry

25   matter to $m^2\ g^{-1}$ C. Observation derived *SLA* for eucalypt is lower than for the other bioenergy crops, and *SLA* for switchgrass is relatively larger. *SLA* is set to the median value of observations for PFT16 (*Miscanthus*) and PFT17 (switchgrass), and close to the 75th percentile value of the data we compiled for PFT14 (eucalypt) and PFT15 (poplar and willow) (Fig. 1d and Table 2).

Another important plant trait for photosynthesis is the leaf orientation, which determines the radiation extinction in the canopy. Although LAI of eucalypts is generally moderate (Anderson, 1981; Stape et al., 2004; Whitehead and Beadle, 2004), leaf angles are nearly close to vertical in mature eucalypts forest (Anderson, 1981; King, 1997), leading to a good distribution of radiation to the lower canopy layers. The light extinction coefficient (*k*) for PFT14 (eucalypt) is therefore set

5   to 0.36 (Table 2) according to the measurement-based estimate by Stape et al. (2004). Similarly, a field study shows the seasonal average *k* ranging from 0.23 to 0.37 for poplars (Ceulemans et al., 1992; Heilman et al., 1996), and a median value of 0.3 was used for PFT15 (Table 2).

2.3.2 Carbon allocation parameters

The maximum carbon allocation to leaf biomass is controlled in ORCHIDEE by a pre-defined maximum LAI value (LAI_{max})

10 beyond which no carbon will be allocated to leaf (Krinner et al., 2005). We adjusted this parameter to match the observed maximum LAI in the field for the four selected bioenergy plants (Table 2). LAI_{max} for PFT14 (eucalypt), PFT15 (poplar and willow), PFT16 (*Miscanthus*) and PFT17 (switchgrass) are set to be 7, 9, 10 and 8, respectively (Ceulemans et al., 1992; Heaton et al., 2008; Heilman et al., 1996; Whitehead and Beadle, 2004; Zub and Brancourt-Hulmel, 2010).

For woody PFTs in ORCHIDEE, the partitioning between aboveground and belowground sapwood biomass is a function of

15 forest age (Krinner et al., 2005):

$$f_{ab,t} = f_{ab,min} + (f_{ab,max} - f_{ab,min}) \times (1 - e^{-t/\tau}) \tag{5}$$

Where $f_{ab,t}$ is the fraction of sapwood allocated to aboveground at age t; $f_{ab,min}$ and $f_{ab,max}$ are the minimum and maximum fraction allocated to aboveground (0.2 and 0.8 respectively); and τ is an empirical parameter. This equation implies that more biomass is allocated to belowground sapwood to develop coarse roots in younger forests. The partition between aboveground

20 and belowground biomass is influenced by resource supply like water and nutrient availability (Litton et al., 2007). For example, belowground carbon allocation in eucalypt is observed to be strongly reduced by irrigation (Barton and Montagu, 2006; Ryan et al., 2010; Stape et al., 2008). Fertilized poplars also showed greater shoot growth than control plots (Coleman et al., 2004). We assumed that bioenergy trees should usually be under intensive management (e.g. irrigation and fertilization) especially in the establishment year (Caslin et al., 2015; Isebrands and Richardson, 2014; Jacobs, 1981). A higher water and

25 nutrient availability then implies a lower investment of biomass on roots for bioenergy trees. In the ORCHIDEE version used here, as there is no specific fertilization or irrigation practice included, the idealized approach chosen to partially account for these managements operations was to reduce τ in Equation (5) from 5 to 2 years (Table 2) to give a maximum allocation of sapwood biomass to aboveground faster than in the standard version. The difference of these two values is illustrated in Fig. S1. Also because the rotation length for bioenergy trees is usually of several years only (Karp and Shield, 2008), it is

30 reasonable to assume that these plants allocate more biomass aboveground in the first few years. However, trees like poplar and willow can sprout from the remaining stem or root (Isebrands and Richardson, 2014), which is not accounted for in the

model. Last, we also adjusted the factor (β, Table 2) in the exponential function to calculate the soil water stress in ORCHIDEE (Krinner et al., 2005; McMurtrie et al., 1990) to reduce the soil moisture stress on bioenergy trees (Fig. S2).

2.3.3 Phenology parameters

An adjustment of parameters related to phenology was performed for the two herbaceous bioenergy PFTs (PFT16 and PFT17, Table 2) to derive the total biomass production for the whole growing season. Lewandowski et al. (2003) and Zub and Brancourt-Hulmel (2010) reviewed growth temperature and growing season length of *Miscanthus* and switchgrass, and found that these two crops have higher cold tolerance and a longer growing season than grasses. Compared to maize, *Miscanthus* has an earlier leaf onset and later leaf fall, and thus its growing season length is 59% longer (Dohleman and Long, 2009). Some *Miscanthus* genotypes need fewer cumulative degree-days for shoot emergence (60 to 118 degree days) and a high frost tolerance (-9 to -6 ℃) (Farrell et al., 2006). To account for this frost tolerance and longer growing season, we decreased the growing degree days for leaf onset in the model (GDD_{onset}) from 700 (standard value for C4 crop PFT) to 320 degree days (same as the default value for C4 grass PFT in ORCHIDEE) and the critical temperature for leaf senescence ($T_{senescence}$) from 10 to 0 ℃ for PFT16 and PFT17 (Table 2). Note that we did not set $T_{senescence}$ to be -9 to -6 ℃, because frost tolerance was only documented for certain *Miscanthus* genotypes, so we used a conservative value of 0 ℃ for *Miscanthus* and switchgrass PFTs. In addition, we increased the critical leaf age beyond which leaves enter senescence (t_{leaf}) and the minimum leaf age to allow leaf senescence ($t_{leaf,min}$) to be the same as the default values for C4 grass PFT (PFT11 in Table 1) in ORCHIDEE (Table 2).

2.3.4 Biomass harvest

The harvest index (*HI*) determines how much aboveground biomass is harvested. Theoretically, all the aboveground biomass of a lingocellulosic crop can be used for energy production. Some IAMs (e.g. GCAM3.0, Kyle et al., 2011) indeed assume a *HI* of 1 for switchgrass for instance. In practice, harvesting of *Miscanthus* and switchgrass is usually performed in winter and early spring after drying and nutrient recycling through leaf falling off (Lewandowski et al., 2003; Zub and Brancourt-Hulmel, 2010) which leads to a lower biomass at harvest. For bioenergy trees, current harvesting techniques can hardly harvest 100% of aboveground biomass (Caslin et al., 2015; Isebrands and Richardson, 2014; Jacobs, 1981). Following Caslin et al. (2010), Richards et al. (2017), and Zhuang et al. (2013), we used a *HI* of 0.9 (i.e. 90% aboveground biomass is harvested) for all the bioenergy PFTs in ORCHIDEE (Table 2). However, for simulations using future land use maps generated from IAMs, we would recommend to set the *HI* same as in IAMs to be consistent.

The rotation length for eucalypt, poplar and willow varies among different tree types, species, locations and plantation purposes (Caslin et al., 2015; Isebrands and Richardson, 2014; Karp and Shield, 2008; Keoleian and Volk, 2005; Mead et al., 2001). For example, eucalypt and poplar for sawlog and veneer utilization are often on rotations of 8-20 years, depending on regions (Isebrands and Richardson, 2014; Mead et al., 2001). But short rotation coppice bioenergy plantation of poplar and

willow have shorter cutting cycles of 3-5 years (Caslin et al., 2015; Isebrands and Richardson, 2014; Karp and Shield, 2008; Keoleian and Volk, 2005). A rotation length of 8 years was used in LPJml model for bioenergy trees (Beringer et al., 2011). In ORCHIDEE, the rotation length for bioenergy tree PFTs is associated with the setting of age classes (see **Section 2.2**). Namely, harvesting starts from the second youngest age class, thus the biomass class boundary for the second youngest forest age cohort is assumed to define the rotation length. For idealized simulations presented below, we used a rotation length of 4-6 years based on the harvest age and rotation length in the evaluation dataset (Fig. 2; **Section 3.2**). Here, the harvest age (Fig. 2) represents the age when the biomass of bioenergy trees was harvested or estimated. It is directly reported by the original literature and corresponding to the reported yield. Rotation length (Fig. 2) is the management practice reported in the original literature, and it is the same as harvest age in most studies. In other studies, however, some trees may be harvested earlier or later than the regular rotation length, e.g. for a comparison purpose. In addition, not all literature reported both harvest age and rotation length (see the number of observations in Fig. 2).

3 Model evaluation

3.1 Evaluation dataset

We used the global bioenergy crop yield dataset from Li et al., (submitted, see **Data availability**) to evaluate the performance of the modified ORCHIDEE-MICT-BIOENERGY model. This global dataset was compiled from more than 200 field measurement based studies with five main bioenergy crop types, i.e. eucalypt, poplar, willow, *Miscanthus* and switchgrass (Li et al., submitted). About 98% of the compiled observations are reported as the aboveground biomass, and the rest are reported as the total of aboveground and belowground biomass. We thus didn't exclude the observations of the total biomass in the model-observation comparison since their fraction is very low (<2%). The biomass yield in this dataset is compiled in a unit of ton DM (dry matter) ha^{-1} yr^{-1}, corresponding to the mean annual biomass yield. For example, if the original literature reported the total harvested biomass of poplar at a certain age, the total biomass amount is divided by age to get the mean annual biomass yield. If the original literature reported the annual harvested biomass of *Miscanthus* for several years, each annual yield is taken as one observation. Note that this dataset does not distinguish the utilization of the plantation (for bioenergy use or for timber / pulpwood). In order to evaluate the simulated biomass yields by ORCHIDEE at half-degree resolution, we calculated the median and range of all observations in each half-degree grid cell containing at least a site of the dataset. Each half-degree grid cell may contain observations from different sites or one site with different species, genotypes, treatments (e.g. different irrigation or fertilization levels). Globally, the number of half-degree grid cells containing observations for PFT14 (eucalypt), PFT15 (poplar and willow), PFT16 (*Miscanthus*) and PFT17 (switchgrass) are 63, 120, 69 and 44 respectively (see maps in **Section 3.5**), giving a total of 296 grid cells (some may be have several crops in common).

3.2 Simulation set-up

The set-up for the site-scale simulations in ORCHIDEE-MICT-BIOENERGY is as follows. The model is forced with 30 min time step climatic forcing data, CRU-NCEP v7 (Viovy, 2017) recycling the period of 1990-2000. The CRU-NCEP forcing data is a merged product of CRU TS climate dataset (Harris et al., 2014) and NCEP reanalysis data (Kalnay et al., 1996). Some observation sites have reported mean annual temperature (MAT) and precipitation (MAP), and we verified that these

5   data are consistent with the MAT and MAP from the CRU-NCEP v7 climate forcing data we used (Fig. S3). Thus no bias correction was applied to the CRU-NCEP v7 climate forcing. The soil texture map used in the model is based on the twelve USDA texture classes from Reynolds et al. (2000).

We assumed a homogenous coverage (100%) of one single bioenergy crop PFT in a grid cell covered by the same PFT type as the site observations. We set an annual harvest fraction of 1% of the grid cell each year. The 1% annual harvest fraction is

10 just an artificial value to make sure that there is always forest in second youngest age class available for harvest every year after a stable rotation is established. We compared the annual harvested biomass in bioenergy harvest pool in per area unit, so the harvest area has no influence on our model evaluation. For the bioenergy trees (PFT14 and PFT15), a spin-up of 100 years without harvest was run first to derive biomass evolution in time to define the respective biomass boundaries for age classes in each grid cell (see Yue et al., 2017). The biomass boundaries are grid-cell specific because of the different

15 vegetation growth rates in different grid cells. The six age classes from youngest to oldest are thus set to be corresponding to 0-4, 4-6, 6-10, 10-30, 30-50, and >50 years. We set the second youngest age class that is used in priority for bioenergy harvest (**Section 2.2**) to be 4-6 years (Fig. 2) based on harvest age and rotation length reported by the original publications in the evaluation dataset (Li et al., submitted). After spin-up, the simulations for PFT14 (eucalypt) and PFT15 (poplar and willow) were run with bioenergy harvest process for 50 years because we only harvested the second age class (4-6 yr) and 50

20 years is long enough to establish a stable rotation. The harvested biomass amount for the last 10 years was used to calculate the median and range of the simulated yields. We divided the harvested biomass by 5 years (4-6 years in the second youngest age class) to obtain the annual mean yields of PFT14 (eucalypt) and PFT15 (poplar and willow). A carbon-to-dry-matter ratio of 0.5 was used to convert the unit of yields into ton DM ha^{-1} yr^{-1}.

For the bioenergy grasses (PFT16 and PFT17) simulations were performed directly (without spin-up) with harvest for 50

25 years, and similarly, the yields of the last 10 years were used for comparison with site observed values. Note that we aim to assess the performance of simulated biomass yields rather than the state of the carbon pools including litter and soil organic matter, that depend on site history. As litter and soil carbon pools do not influence vegetation productivity in the model, we did not perform a full long spin-up of carbon pools to their equilibrium values.

3.3 Simulated bioenergy yields at global level

30 The simulated bioenergy biomass yields in comparison with field observations for the four bioenergy crops are shown in Fig. 3. The model-observation results generally lie around the 1:1 ratio line (Fig. 3 left panel). Although there are some large overestimates and underestimates especially for PFT14 (eucalypt) and PFT16 (*Miscanthus*), no systematic bias was found

for all bioenergy crop PFTs. ORCHIDEE-MICT-BIOENERGY reproduces the frequency distributions of the observed biomass yields across different grid cells well (Fig. 3 right panel). The median observed and simulated biomass yields in all grid cells are 16.0 and 17.5 ton DM ha^{-1} yr^{-1} for PFT14 (eucalypt), 8.4 and 8.3 ton DM ha^{-1} yr^{-1} for PFT15 (poplar and willow), 12.7 and 10.8 ton DM ha^{-1} yr^{-1} for PFT16 (*Miscanthus*), and 8.7 and 9.0 ton DM ha^{-1} yr^{-1} for PFT17 (switchgrass), respectively. PFT14 (eucalypt) shows a large spread both in the observed and simulated biomass yields. Some site observation data with high yield (>25 ton DM ha^{-1} yr^{-1}) were not reproduced by the model for eucalypt. By contrast, observed and simulated yields for PFT15 (poplar and willow) and PFT17 (switchgrass) concentrate in a relatively narrow range.

It should be noted that it is impossible to perfectly reproduce observations in all grid cells, i.e. all dots in Fig. 3 on the 1:1 line, because of uncertainties in the observation dataset, e.g. treatments, genotypes, and local fertilization or irrigation practices as well as in soil characteristics and climate forcing variations prescribed in the model. The error bars of modelled yield (y-axis) come from the range of different harvest years and represents inter annual variability. The error bars of the observations (x-axis) represent the range from different sites, crop species, genotypes and treatments as well as the observation number in each grid cell. It is difficult to systematically synthesize all these factors to give an optimal observed yield in each grid cell. First, different species and genotypes are impossible to be accounted for in a global vegetation model, and thus a further classification of such information would not help the model evaluation. Second, some management practices are difficult to quantify. For example, some studies reported the irrigation as amount per year while some others reported like "irrigating when necessary". The fertilization rates are also difficult to synthesize between different studies because they applied different types of fertilizers, some annually but some in random years. Third, each observation is associated with different managements / treatments, and there is no uniform standard to weight all these different managements. Last, global vegetation models usually run at a half-degree resolution, which may not fully represent the site level climate variations and soil properties. However, the error bars for most sites (67%, 73%, 74% and 64% for PFT14 to PFT17 respectively) reach the 1:1 line (Fig. 3 left panel), implying that the model is able to capture at least some observations in these grid cells.

3.4 Biomass-age relationship at site level

A good representation of biomass-age curves for bioenergy trees in the model is crucial to reproduce the yields, especially in the first several years after plantation (≤ rotation length). However, most of the observations in the global evaluation dataset were only mean annual yield (Li et al., submitted). This precludes a detailed analysis of biomass dynamics over time for bioenergy trees. We thus selected 22 studies (Table S2) from the evaluation dataset that reported biomass amount of multiple ages (at least two years) and at the same site for eucalypt, poplar or willow. We went through the original articles to derive the biomass-age curves and compared them with the same curves from the model simulations (Fig. 4 and Fig. 5).

There is a good agreement on biomass-age relationship of eucalypt between model and observation in some sites in Australia and China (Site #2, #8-12 in Fig. 4). But the model underestimates the biomass evolution of eucalypt at Site #13 in New Zealand and overestimates it at Site #5-6 in China (Fig. 4). For poplar and willow, there are two long-term (>10 yr) consecutive observation sites in Wisconsin, USA (Site #13 and #15 in Fig. 5), where the model captures the biomass-age

5 relationship well. In some other sites (Site #2, #3, #7, #14 and #17 in Fig. 5), however, the model results only agree with observations for the first few years and then deviate from the observations afterwards. The model generally coarsely underestimates the biomass of poplar and willow at all ages in the sites in eastern (Site #1 in Fig. 5) and western (Site #5 and #6 in Fig. 5) coastal region of US, in UK (Site #8 to #11 in Fig. 5) and in Sweden (Site #16 in Fig. 5), but overestimates in India (Site #12 in Fig. 5) and at one site in China (Site #18 in Fig. 5).

10 Possible reasons for the model-observation differences at each site using the information reported in the original studies (see details in Table S2) include the different varieties of species (e.g. genotypes) and management (e.g. fertilization, irrigation or spacing) in the field, which were not explicitly considered in the model. For example, the model overestimates biomass at Site #4 in Fig. 4 because of the large spacing of plantation the trial experiment (Han et al., 2010) which results in lower biomass yield when converting the unit of ton DM plant^{-1} yr^{-1} to ton DM ha^{-1} yr^{-1}. Site #13, #14 and #15 in Fig. 5 are from

15 the same study (Strong and Hansen, 1993), and the model reproduces at Site #13 and #15 but underestimates it at Site #14. It is because the biomass-age curves at Site #13 and #15 are from the average of several genotypes (some have higher yields and some lower), but only one genotype with relatively high yield was planted at Site #14 (Strong and Hansen, 1993), causing an model underestimation at Site #14. In addition, our model seems to systematically underestimate biomass production of willow for the sites in UK (Site #8-11 in Fig. 5). These observed biomass production in UK was based on a

20 range of willow varieties in trial experiments, and the authors (Lindegaard et al., 2011) claimed that the trial experiments generate higher yields than large-scale commercial plantations because of the differences in land quality and practice guidelines (e.g. cutting, harvest index). Despite of some model-observation differences, we emphasized that the modeled biomass-age curves are consistent with observations for most sites within the rotation length.

3.5 Maps of differences between simulated and observed yields

25 The spatial distributions of relative differences between simulated and observed biomass yields are shown in Fig. 6 to Fig. 9 for each PFT. The observations for eucalypt mainly distribute in Brazil, tropical Africa, South Asia and Australia (Fig. 6). ORCHIDEE-MICT-BIOENERGY slightly underestimates biomass yield for PFT14 (eucalypt) in Brazil and overestimates some grid cells in southern China and Australia. Some biomass observations of eucalypts in Australia are obtained from native forests (Li et al., submitted), which may partly explain the overestimation by model.

30 Poplar and willow are mainly planted in temperate regions like the United States, Europe, and Central and East Asia (Fig. 7). ORCHIDEE-MICT-BIOENERGY underestimates the biomass yields for PFT15 (poplar and willow) in western US but overestimates the yields in eastern US. There is no distinct pattern for the differences between observations and model

results in Europe with both underestimation and overestimation across grid cells. But it seems that the simulated biomass yields are lower than observations in Sweden. In Central and East Asia, biomass yields in the inland grid cells are generally underestimated but those in the coastal areas are overestimated.

Most of the observations for *Miscanthus* are from Europe although some trial tests are also available in eastern US and a few in China (Fig. 8). In the US, very slight underestimation of yield was found in the inland areas while overestimation was more close to the ocean. The model underestimates biomass yields for PFT16 (*Miscanthus*) in UK and South Europe, and slightly overestimates it in other areas in Europe. There are only three grid cells with *Miscanthus* yield observations in China, and they are all largely overestimated in the simulations.

Switchgrass is a native perennial grass in North America (Lewandowski et al., 2003) and thus mainly grows in US (Fig. 9). There are also very few observations in Europe and East Asia. ORCHIDEE-MICT-BIOENERGY can generally reproduce the biomass yields for PFT17 (switchgrass) in central US but overestimate in eastern US, especially in some grid cells around the Great Lakes. The simulated biomass yields are lower than observations in grid cells in Europe and China but fit well with observations in the grid cell in Japan.

4 Discussion

4.1 Model-observation difference in different climate bins

The differences between simulated and observed biomass yields for bioenergy crop PFTs in different MAT and MAP intervals are shown in Fig. 10. There is no systematic bias of simulated biomass yields in the climate space except in the climate zones with relatively high MAT and MAP (upper-right grids in Fig. 10b,c) for PFT15 (poplar and willow) to PFT17 (switchgrass). For these PFTs, It seems ORCHIDEE overestimated the yields with MAT > 15 °C and MAP > 1000 mm yr^{-1}.

The distribution patterns in Fig. 10 also reflect the different climate conditions of growth for these bioenergy crops. Consistent with their physiological characteristics, eucalypts grow in tropical regions (Fig. 6) with MAT > 10 °C and MAP > 500 mm yr^{-1} (Fig. 10). By contrast, poplars and willows grow in temperate regions (Fig. 7) and some under low MAT and MAP (Fig. 10). *Miscanthu*s and switchgrass are usually planted in Europe and US (Fig. 8 and Fig. 9) with moderate MAT and MAP.

We further investigated whether other climate forcing variables in the model impact the model-observation differences using the multiple linear regression method (Table S3) and the regression tree method (Breiman et al., 1984; Pedregosa and Varoquaux, 2011) (Fig. S4). In these two methods, PFT types and nine climate forcing variables (Table S3) were used as independent variables and the relative model-observation difference as dependent variable. The multiple linear regression is non-significant (p = 0.28) with a very low r^2 (0.01), suggesting that the variations in the relative model-observation

differences is mostly explained by other factors rather than the climate forcing biases used in the model. In the regression tree (Fig. S4), the first discriminator is short-wave radiation but it only split very few samples. Although north wind speed separates a relatively large proportion of samples (Fig. S4), it has little to do with the biomass production in the model. Therefore, results from these two regression methods suggest the model-observation biases are unlikely caused by the model

5   simulation.

4.2 Model performance before and after bioenergy crop implementation

In this study, we added four new PFTs to represent the main lignocellulosic bioenergy crops and implemented new parameterizations for each new PFT. As a first step, we evaluated the biomass production from bioenergy crops in ORCHIDEE using a global field measurement dataset. We compared the biomass yields simulated by the new ORCHIDEE-

10   MICT-BIOENERGY with the yields from previous ORCHIDEE version (Fig. 11). In the previous version, bioenergy crops were all taken as herbaceous C4 crop (PFT13), and thus severe overestimation (overestimating 60% on average) occurs for tropical bioenergy trees (i.e. eucalypts, gray squares in Fig. 11a). Although using herbaceous C4 crop generally reproduce the observed biomass yields of poplars and willows (grey squares in Fig. 11b), different carbon dynamics in litter and soil and water and energy balance can be expected.

15   Using the right tree PFTs for bioenergy trees and right herbaceous PFTs for bioenergy grasses but without new parameterizations also results in significant biases in the simulated yields compared to observations (blue triangles in Fig. 11). Specifically, using the default parameters of previous version is found to largely underestimate biomass yields of all bioenergy trees (blue triangles in Fig. 11a,b). For bioenergy grasses, slight underestimation was found for *Miscanthus* (blue triangles in Fig. 11c) while large overestimation was found for switchgrass (blue triangles in Fig. 11d) with previous default

20   parameters. The large biomass yields of C4 crops in previous ORCHIDEE version (blue triangles in Fig. 11c,d) mainly result from the high V_{cmax25} (Table 2), which is not the reason for the high yields of *Miscanthus* and switchgrass (Fig. 1). We emphasize again that different bioenergy crops achieve high productivities through different pathways based on their plant traits (**Section 2.3**) and it is important to specifically consider these traits by proper parameterizations in the global vegetation models.

25   **4.3 Future development**

In ORCHIDEE-MICT-BIOENERGY, nutrient limitations and management like irrigation and fertilization are not explicitly implemented. Instead, we used parameter values in the range that favors a higher productivity (**Section 2.3**, Fig. 1). However, there are still some regional biases of biomass yields for different bioenergy crops. For example, ORCHIDEE-MICT-BIOENERGY underestimates the biomass yields of *Miscanthus* in UK by 43% (Fig. 8) and overestimates the yields of

30   switchgrass in eastern US by 18% (Fig. 9). Thus, for a regional use of modelled results, slight modifications of related parameters would be needed.

In addition to the biomass yields, the carbon densities or fluxes in soil should also be systematically evaluated, which is currently impeded by lack of a global dataset of soil organic carbon for bioenergy crops to our knowledge. For a long-term perspective, the implementation of explicit managements and interactions between bioenergy yields and nutrient limitations are increasingly important to simulate carbon reduction potentials of bioenergy crop deployments.

5 Beside the biogeochemical processes, it is also critical to further parameterize and evaluate biophysical processes, especially in the coupled simulations of global vegetation models with climate models to calculate the biophysical feed-backs. Field measurements on e.g. leaf traits, heat exchange and transpiration of bioenergy crops extend our knowledge of these biophysical processes and need to be integrated adequately in the global vegetation models.

5 Conclusions

10 Bioenergy crop has been extensively assumed in IAMs and is an important type of future land use. However, most global vegetation models do not have specific representations of these bioenergy crops. It is important to accurately represent the physiology, phenology and carbon allocation of these crops because it fundamentally impacts the hydrology dynamics, energy balance and carbon cycle. Especially for woody bioenergy crops like eucalypts, poplars and willows, not only the biomass yields but also the seasonal variations and biophysical effects, and carbon turnover are impacted by new

15 parameterizations.

In this study, we demonstrated the importance of proper representative of bioenergy crops in a global vegetation model to reproduce the observation-based biomass yields. We introduced new bioenergy crop PFTs based on their plant characteristics, modified the parameters relevant to productivity based on field measurements and empirical evidence, and added the dedicated harvest process to simulate bioenergy biomass yields. The bioenergy crop simulations in ORCHIDEE-

20 MICT-BIOENERGY generally reproduced the observation-based biomass yields for bioenergy crops at global level. However, it is still difficult to match observations site-by-site due to the uncertainties in the observation dataset and the lack of explicit managements in the model. Evaluations on soil carbon dynamics and biophysical variables are further needed. Our work improves the performance of ORCHIDEE on bioenergy crops modelling, and the parameters used in ORCHIDEE-MICT-BIOENERGY also provide guidance for other vegetation models on incorporating dedicated bioenergy crops.

6 Code availability

25

This model development is based on ORCHIDEE-MICT version (Guimberteau et al., 2017) with gross land use changes and forest age dynamics (Yue et al., 2017). The code availability can be found in these two publications. The newly implemented parameterization can be found in Table 2 in this study. The source code of this version (ORCHIDEE-MICT-BIOENERGY) is available online (http://forge.ipsl.jussieu.fr/orchidee/browser/perso/wei.li/ORCHIDEE_GLUC_BIOENERGY), but its

access is restricted to registered users. Request can be sent to the corresponding author for a username and password for code access. ORCHIDEE-MICT is governed by the CeCILL license under French law and abiding by the rules of distribution of free software. One can use, modify and/or redistribute the software under the terms of the CeCILL license as circulated by CEA, CNRS and INRIA at the following URL: http://www.cecill.info.

7 Data availability

The compiled V_{cmax} and J_{max} data from observations can be found in supplementary Table S1. The evaluation dataset used in this study i.e. the global yield dataset for major lignocellulosic bioenergy crops based on field measurements, has been submitted to a data description journal and will be freely accessed after the acceptance of the data description paper.

Reference

Alexandratos, N. and Bruinsma, J.: World agriculture towards 2030/2050: the 2012 revision, ESA Working paper Rome, FAO., 2012.

Anderson, M. C.: The geometry of leaf distribution in some south-eastern Australian forests, Agric. Meteorol., 25, 195–206, 1981.

Barton, C. V. M. and Montagu, K. D.: Effect of spacing and water availability on root: shoot ratio in Eucalyptus camaldulensis, Forest Ecol. Manag., 221(1), 52–62, 2006.

Beringer, T. I. M., Lucht, W. and Schaphoff, S.: Bioenergy production potential of global biomass plantations under environmental and agricultural constraints, GCB Bioenergy, 3(4), 299–312, 2011.

Bonsch, M., Humpenöder, F., Popp, A., Bodirsky, B., Dietrich, J. P., Rolinski, S., Biewald, A., Lotze-Campen, H., Weindl, I. and Gerten, D.: Trade-offs between land and water requirements for large-scale bioenergy production, Gcb Bioenergy, 8(1),

Geoscientific
Model Development
Discussions

11–24, 2016.

Bonsch, M., Popp, A., Biewald, A., Rolinski, S., Schmitz, C., Weindl, I., Stevanovic, M., Högner, K., Heinke, J. and Ostberg, S.: Environmental flow provision: Implications for agricultural water and land-use at the global scale, Glob. Environ. Chang., 30, 113–132, 2015.

5   Bouwman, A. F., Kram, T. and Klein Goldewijk, K.: Integrated modelling of global environmental change, An Overv. IMAGE, 2(4), 225–228, 2006.

Breiman, L., Friedman, J. H., Olshen, R. A. and Stone, C. J.: Classification and Regression Trees., 1984.

Brovkin, V., Boysen, L., Arora, V. K., Boisier, J. P., Cadule, P., Chini, L., Claussen, M., Friedlingstein, P., Gayler, V. and Van Den Hurk, B.: Effect of anthropogenic land-use and land-cover changes on climate and land carbon storage in CMIP5
10   projections for the twenty-first century, J. Clim., 26(18), 6859–6881, 2013.

Cadoux, S., Riche, A. B., Yates, N. E. and Machet, J.-M.: Nutrient requirements of Miscanthus x giganteus: conclusions from a review of published studies, Biomass and Bioenergy, 38, 14–22, 2012.

Caslin, B., Finnan, J. and McCracken, A.: Short rotation coppice willow best practice guidelines, Teagas AFBI, Belfast, 2010.

15   Caslin, B., Finnan, J. and McCracken, A.: Short Rotation coppice willow—best practice guidelines. Teagasc, Crops Research Centre, Oak Park, Carlow, Ireland, 2015.

Ceulemans, R., Impens, I., Mau, F., Van Hecke, P. and Chen, S.: Dry mass production and solar radiation conversion efficiency of poplar clones, in Biomass for energy, industry and environment/Grassi, G.[edit.], pp. 157–163., 1992.

Chang, J., Ciais, P., Viovy, N., Vuichard, N., Sultan, B. and Soussana, J.: The greenhouse gas balance of European
20   grasslands, Global Chang. Biol., 21(10), 3748–3761, 2015.

Coleman, M. D., Friend, A. L. and Kern, C. C.: Carbon allocation and nitrogen acquisition in a developing Populus deltoides plantation, Tree Physiol., 24(12), 1347–1357, 2004.

Dohleman, F. G., Heaton, E. A., Leakey, A. D. B. and Long, S. P.: Does greater leaf-level photosynthesis explain the larger solar energy conversion efficiency of Miscanthus relative to switchgrass?, Plant. Cell Environ., 32(11), 1525–1537, 2009.

25   Dohleman, F. G. and Long, S. P.: More productive than maize in the Midwest: how does Miscanthus do it?, Plant Physiol., 150(4), 2104–2115, 2009.

Farquhar, G. D. v, von Caemmerer, S. von and Berry, J. A.: A biochemical model of photosynthetic CO_2 assimilation in

leaves of C3 species, Planta, 149(1), 78–90, 1980.

Farrell, A. D., Clifton-Brown, J. C., Lewandowski, I. and Jones, M. B.: Genotypic variation in cold tolerance influences the yield of Miscanthus, Ann. Appl. Biol., 149(3), 337–345, 2006.

Forrester, D. I.: Growth responses to thinning, pruning and fertiliser application in Eucalyptus plantations: a review of their
5   production ecology and interactions, Forest Ecol. Manag., 310, 336–347, 2013.

Fuss, S., Canadell, J. G., Peters, G. P., Tavoni, M., Andrew, R. M., Ciais, P., Jackson, R. B., Jones, C. D., Kraxner, F. and Nakicenovic, N.: Betting on negative emissions, Nat. Clim. Chang., 4(10), 850–853, 2014.

Gerland, P., Raftery, A. E., Ševčíková, H., Li, N., Gu, D., Spoorenberg, T., Alkema, L., Fosdick, B. K., Chunn, J. and Lalic, N.: World population stabilization unlikely this century, Science (80-.)., 346(6206), 234–237, 2014.

10   Guimberteau, M., Zhu, D., Maignan, F., Huang, Y., Yue, C., Dantec-Nédélec, S., Ottlé, C., Jornet-Puig, A., Bastos, A., Laurent, P., Goll, D., Bowring, S., Chang, J., Guenet, B., Tifafi, M., Peng, S., Krinner, G., Ducharne, A., Wang, F., Wang, T., Wang, X., Wang, Y., Yin, Z., Lauerwald, R., Joetzjer, E., Qiu, C., Kim, H. and Ciais, P.: ORCHIDEE-MICT (revision 4126), a land surface model for the high-latitudes: model description and validation, Geosci. Model Dev. Discuss., 1–65, doi:10.5194/gmd-2017-122, 2017.

15   Han, F., Zhou, Q. and Chen, S.: Effects of density on growth of Eucalypt bio-energy plantations in Leizhou Peninsula, J. Trop. Subtrop. Bot., 18(4), 350–356, [in Chinese], 2010.

Harris, I., Jones, P. D., Osborn, T. J. and Lister, D. H.: Updated high-resolution grids of monthly climatic observations - the CRU TS3.10 Dataset, Int. J. Climatol., 34(3), 623–642, doi:10.1002/joc.3711, 2014.

Heaton, E. A., Dohleman, F. G. and Long, S. P.: Meeting US biofuel goals with less land: the potential of Miscanthus,
20   Global Chang. Biol., 14(9), 2000–2014, 2008.

Heck, V., Gerten, D., Lucht, W. and Boysen, L. R.: Is extensive terrestrial carbon dioxide removal a "green" form of geoengineering? A global modelling study, Glob. Planet. Change, 137, 123–130, doi:10.1016/j.gloplacha.2015.12.008, 2016.

Heilman, P. E., Hinckley, T. M., Roberts, D. A. and Ceulemans, R.: Production physiology, Biol. Popul. its Implic. Manag. Conserv., (Part II), 459–489, 1996.

25   Isebrands, J. G. and Richardson, J.: Poplars and willows: trees for society and the environment, CABI., 2014.

Jacobs, M. R.: Eucalypts for planting., Food and agriculture organization of the United Nations., 1981.

Kalnay, E., Kanamitsu, M., Kistler, R., Collins, W., Deaven, D., Gandin, L., Iredell, M., Saha, S., White, G., Woollen, J.,

Zhu, Y., Chelliah, M., Ebisuzaki, W., Higgins, W., Janowiak, J., Mo, K. C., Ropelewski, C., Wang, J., Leetmaa, A., Reynolds, R., Jenne, R. and Joseph, D.: The NCEP/NCAR 40-year reanalysis project, Bull. Am. Meteorol. Soc., 77(3), 437–471, doi:10.1175/1520-0477(1996)077<0437:TNYRP>2.0.CO;2, 1996.

Karp, A. and Shield, I.: Bioenergy from plants and the sustainable yield challenge, New Phytol., 179(1), 15–32, 2008.

5   Kattge, J. and Knorr, W.: Temperature acclimation in a biochemical model of photosynthesis: a reanalysis of data from 36 species, Plant. Cell Environ., 30(9), 1176–1190, 2007.

Keoleian, G. A. and Volk, T. A.: Renewable energy from willow biomass crops: life cycle energy, environmental and economic performance, BPTS, 24(5–6), 385–406, 2005.

King, D. A.: The functional significance of leaf angle in Eucalyptus, Aust. J. Bot., 45(4), 619–639, 1997.

10 Klein, D., Luderer, G., Kriegler, E., Strefler, J., Bauer, N., Leimbach, M., Popp, A., Dietrich, J. P., Humpenöder, F. and Lotze-Campen, H.: The value of bioenergy in low stabilization scenarios: an assessment using REMIND-MAgPIE, Clim. Change, 123(3–4), 705–718, 2014.

Krinner, G., Viovy, N., de Noblet-Ducoudré, N., Ogée, J., Polcher, J., Friedlingstein, P., Ciais, P., Sitch, S. and Prentice, I. C.: A dynamic global vegetation model for studies of the coupled atmosphere-biosphere system, Global Biogeochem. Cycles,
15 19(1), n/a-n/a, doi:10.1029/2003GB002199, 2005.

Kyle, P., Luckow, P., Calvin, K., Emanuel, W., Nathan, M. and Zhou, Y.: GCAM 3.0 agriculture and land use: data sources and methods, Pacific Northwest Natl. Lab. PNNL-21025. http//wiki. umd. edu/gcam/images/2/25/GCAM_AgLU_Data_Documentation. pdf, 2011.

Laurent, A., Pelzer, E., Loyce, C. and Makowski, D.: Ranking yields of energy crops: a meta-analysis using direct and
20 indirect comparisons, Renew. Sustain. energy Rev., 46, 41–50, 2015.

LeBauer, D., Dietze, M., Kooper, R., Long, S. P., Mulrooney, P., Rhode, G. S. and Wang, D.: Biofuel Ecophysiological Traits and Yields Database (BETYdb), Energy Biosci. Institute, Univ. Illinois Urbana-Champaign, Urbana, IL, USA, 2010.

Lewandowski, I., Scurlock, J. M. O., Lindvall, E. and Christou, M.: The development and current status of perennial rhizomatous grasses as energy crops in the US and Europe, Biomass and bioenergy, 25(4), 335–361, 2003.

25 Li, W., Ciais, P. and Peng, S.: A global dedicated bioenergy crop yields dataset based on field measurements, , submitted, 2017.

Lindegaard, K. N., Carter, M. M., McCracken, A., Shield, I., MacAlpine, W., Jones, M. H., Valentine, J. and Larsson, S.: Comparative trials of elite Swedish and UK biomass willow varieties 2001–2010, Asp Appl Biol, 112(57), e66, 2011.

Litton, C. M., Raich, J. W. and Ryan, M. G.: Carbon allocation in forest ecosystems, Global Chang. Biol., 13(10), 2089–2109, 2007.

McCalmont, J. P., Hastings, A., McNamara, N. P., Richter, G. M., Robson, P., Donnison, I. S. and Clifton-Brown, J.: Environmental costs and benefits of growing Miscanthus for bioenergy in the UK, GCB Bioenergy, 9(3), 489–507, 2017.

5   McMurtrie, R. E., Rook, D. A. and Kelliher, F. M.: Modelling the yield of Pinus radiata on a site limited by water and nitrogen, Forest Ecol. Manag., 30(1–4), 381–413, doi:10.1016/0378-1127(90)90150-A, 1990.

Mead, D. J., Ugalde, L. and Perez, O.: Mean annual volume increment of selected industrial forest plantation species., 2001.

Medlyn, B. E., Dreyer, E., Ellsworth, D., Forstreuter, M., Harley, P. C., Kirschbaum, M. U. F., Le Roux, X., Montpied, P., Strassemeyer, J. and Walcroft, A.: Temperature response of parameters of a biochemically based model of photosynthesis. II.

10   A review of experimental data, Plant. Cell Environ., 25(9), 1167–1179, 2002.

Meier, P. J., Cronin, K. R., Frost, E. A., Runge, T. M., Dale, B. E., Reinemann, D. J. and Detlor, J.: Potential for electrified vehicles to contribute to US petroleum and climate goals and implications for advanced biofuels, Environ. Sci. Technol., 49(14), 8277–8286, 2015.

Melillo, J. M., Reilly, J. M., Kicklighter, D. W., Gurgel, A. C., Cronin, T. W., Paltsev, S., Felzer, B. S., Wang, X., Sokolov,

15   A. P. and Schlosser, C. A.: Indirect emissions from biofuels: how important?, Science (80-.)., 326(5958), 1397–1399, 2009.

Miguez, F. E., Villamil, M. B., Long, S. P. and Bollero, G. A.: Meta-analysis of the effects of management factors on Miscanthus×giganteus growth and biomass production, Agric. For. Meteorol., 148(8), 1280–1292, 2008.

Pedregosa, F. and Varoquaux, G.: Scikit-learn: Machine learning in Python., 2011.

Piao, S., Ciais, P., Friedlingstein, P., de Noblet-Ducoudré, N., Cadule, P., Viovy, N. and Wang, T.: Spatiotemporal patterns

20   of terrestrial carbon cycle during the 20th century, Global Biogeochem. Cycles, 23(4), doi:10.1029/2008GB003339, 2009.

Popp, A., Dietrich, J. P., Lotze-Campen, H., Klein, D., Bauer, N., Krause, M., Beringer, T., Gerten, D. and Edenhofer, O.: The economic potential of bioenergy for climate change mitigation with special attention given to implications for the land system, Environ. Res. Lett., 6(3), 34017, 2011.

Popp, A., Rose, S. K., Calvin, K., Van Vuuren, D. P., Dietrich, J. P., Wise, M., Stehfest, E., Humpenöder, F., Kyle, P. and

25   Van Vliet, J.: Land-use transition for bioenergy and climate stabilization: model comparison of drivers, impacts and interactions with other land use based mitigation options, Clim. Change, 123(3–4), 495–509, 2014.

Reynolds, C. A., Jackson, T. J. and Rawls, W. J.: Estimating soil water-holding capacities by linking the Food and Agriculture Organization soil map of the world with global pedon databases and continuous pedotransfer functions, Water

Resour. Res., 36(12), 3653–3662, doi:10.1029/2000WR900130, 2000.

Richards, M., Pogson, M., Dondini, M., Jones, E. O., Hastings, A., Henner, D. N., Tallis, M. J., Casella, E., Matthews, R. W. and Henshall, P. A.: High-resolution spatial modelling of greenhouse gas emissions from land-use change to energy crops in the United Kingdom, GCB Bioenergy, 9(3), 627–644, 2017.

5 Robertson, G. P., Hamilton, S. K., Barham, B. L., Dale, B. E., Izaurralde, R. C., Jackson, R. D., Landis, D. A., Swinton, S. M., Thelen, K. D. and Tiedje, J. M.: Cellulosic biofuel contributions to a sustainable energy future: Choices and outcomes, Science (80-.)., 356(6345), eaal2324, 2017.

Ryan, M. G., Stape, J. L., Binkley, D., Fonseca, S., Loos, R. A., Takahashi, E. N., Silva, C. R., Silva, S. R., Hakamada, R. E. and Ferreira, J. M.: Factors controlling Eucalyptus productivity: how water availability and stand structure alter production
10 and carbon allocation, Forest Ecol. Manag., 259(9), 1695–1703, 2010.

Searchinger, T., Heimlich, R., Houghton, R. A., Dong, F., Elobeid, A., Fabiosa, J., Tokgoz, S., Hayes, D. and Yu, T.-H.: Use of US croplands for biofuels increases greenhouse gases through emissions from land-use change, Science (80-.)., 319(5867), 1238–1240, 2008.

Smith, P., Davis, S. J., Creutzig, F., Fuss, S., Minx, J., Gabrielle, B., Kato, E., Jackson, R. B., Cowie, A. and Kriegler, E.:
15 Biophysical and economic limits to negative CO2 emissions, Nat. Clim. Chang., 6(1), 42–50, 2016.

Stape, J. L., Binkley, D. and Ryan, M. G.: Eucalyptus production and the supply, use and efficiency of use of water, light and nitrogen across a geographic gradient in Brazil, Forest Ecol. Manag., 193(1), 17–31, 2004.

Stape, J. L., Binkley, D. and Ryan, M. G.: Production and carbon allocation in a clonal Eucalyptus plantation with water and nutrient manipulations, Forest Ecol. Manag., 255(3–4), 920–930, doi:10.1016/j.foreco.2007.09.085, 2008.

20 Stehfest, E., van Vuuren, D., Bouwman, L. and Kram, T.: Integrated assessment of global environmental change with IMAGE 3.0: Model description and policy applications, Netherlands Environmental Assessment Agency (PBL)., 2014.

Strong, T. and Hansen, E.: Hybrid poplar spacing/productivity relations in short rotation intensive culture plantations, Biomass and Bioenergy, 4(4), 255–261, doi:10.1016/0961-9534(93)90083-G, 1993.

United Nations: World Population Prospects: The 2017 Revision, Key Findings and Advance Tables. [online] Available
25 from: https://esa.un.org/unpd/wpp/Publications/Files/WPP2017_KeyFindings.pdf, 2017.

Viovy, N.: CRUNCEP dataset, [online] Available from:
ftp://nacp.ornl.gov/synthesis/2009/frescati/temp/land_use_change/original/readme.htm (Accessed 20 July 2008), 2017.

Wang, D., Maughan, M. W., Sun, J., Feng, X., Miguez, F., Lee, D. and Dietze, M. C.: Impact of nitrogen allocation on

growth and photosynthesis of Miscanthus (Miscanthus×giganteus), Gcb Bioenergy, 4(6), 688–697, 2012.

Whitaker, J., Ludley, K. E., Rowe, R., Taylor, G. and Howard, D. C.: Sources of variability in greenhouse gas and energy balances for biofuel production: a systematic review, Gcb Bioenergy, 2(3), 99–112, 2010.

Whitehead, D. and Beadle, C. L.: Physiological regulation of productivity and water use in Eucalyptus: a review, Forest Ecol.
5   Manag., 193(1), 113–140, 2004.

Wilkenskjeld, S., Kloster, S., Pongratz, J., Raddatz, T. and Reick, C. H.: Comparing the influence of net and gross anthropogenic land-use and land-cover changes on the carbon cycle in the MPI-ESM, Biogeosciences, 11(17), 4817, 2014.

Wullschleger, S. D.: Biochemical limitations to carbon assimilation in C3 plants—a retrospective analysis of the A/Ci curves from 109 species, J. Exp. Bot., 44(5), 907–920, 1993.

10 Yan, J., Zhu, C., Liu, W., Luo, F., Mi, J., Ren, Y., Li, J. and Sang, T.: High photosynthetic rate and water use efficiency of Miscanthus lutarioriparius characterize an energy crop in the semiarid temperate region, Gcb Bioenergy, 7(2), 207–218, 2015.

Yin, X. and Struik, P. C.: C 3 and C 4 photosynthesis models: an overview from the perspective of crop modelling, NJAS-Wageningen J. Life Sci., 57(1), 27–38, 2009.

15 Yin, X. and Struik, P. C.: Can increased leaf photosynthesis be converted into higher crop mass production? A simulation study for rice using the crop model GECROS, J. Exp. Bot., 68(9), 2345–2360, doi:10.1093/jxb/erx085, 2017.

Yue, C., Ciais, P., Luyssaert, S., Li, W., McGrath, M., Chang, J. and Peng, S.: Representing anthropogenic gross land use change, wood harvest and forest age dynamics in a global vegetation model ORCHIDEE-MICT (r4259), Geosci. Model Dev. Discuss., 2017.

20 Zhuang, Q., Qin, Z. and Chen, M.: Biofuel, land and water: maize, switchgrass or Miscanthus?, Environ. Res. Lett., 8(1), 15020, 2013.

Zub, H. W. and Brancourt-Hulmel, M.: Agronomic and physiological performances of different species of Miscanthus, a major energy crop. A review, Agron. Sustain. Dev., 30(2), 201–214, 2010.
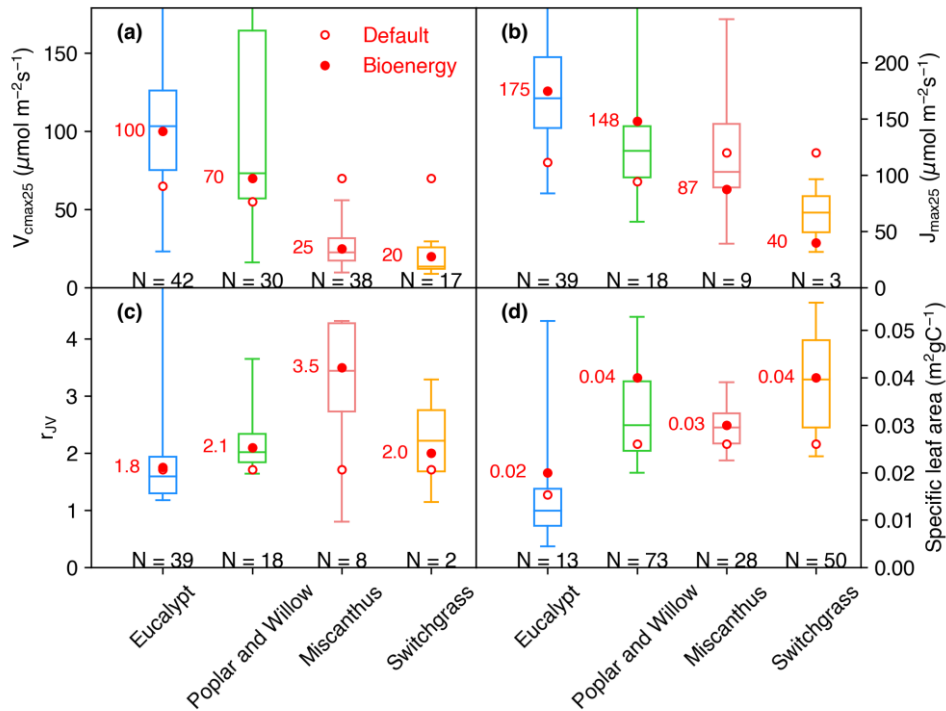
Figure 1 V_{cmax25} (**a**), J_{max25} (**b**), r_{JV25} (V_{cmax25}/J_{max25}, **c**) and specific leaf area (*SLA*, **d**) collected from measurements. The box plot indicates the interquartile range of measurements. The data size of measurements is shown below the box. The default values (open circles) and adjusted values (filled circles) for bioenergy crops are also shown. Because the model does not prescribe J_{max25} but rather calculates it from V_{cmax25}, J_{max25} values for ORCHIDEE shown here (circles in b) are calculated by $V_{cmax25} \times r_{JV}$ (circles in a and b).
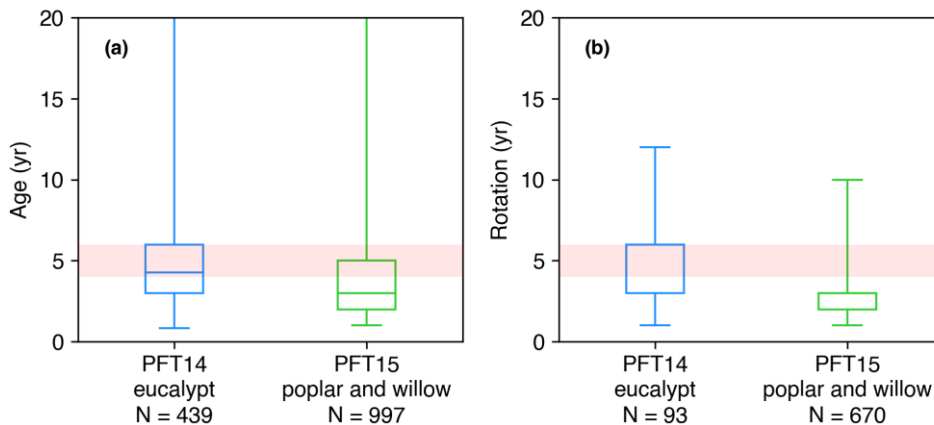
Figure 2 Harvest age (**a**) and rotation length (**b**) in the evaluation dataset. The box plot indicates the interquartile range, and number of observations is also shown. In this study, the harvest age class is set to be 4-6 years (red shade).

Geoscientific
Model Development
Discussions
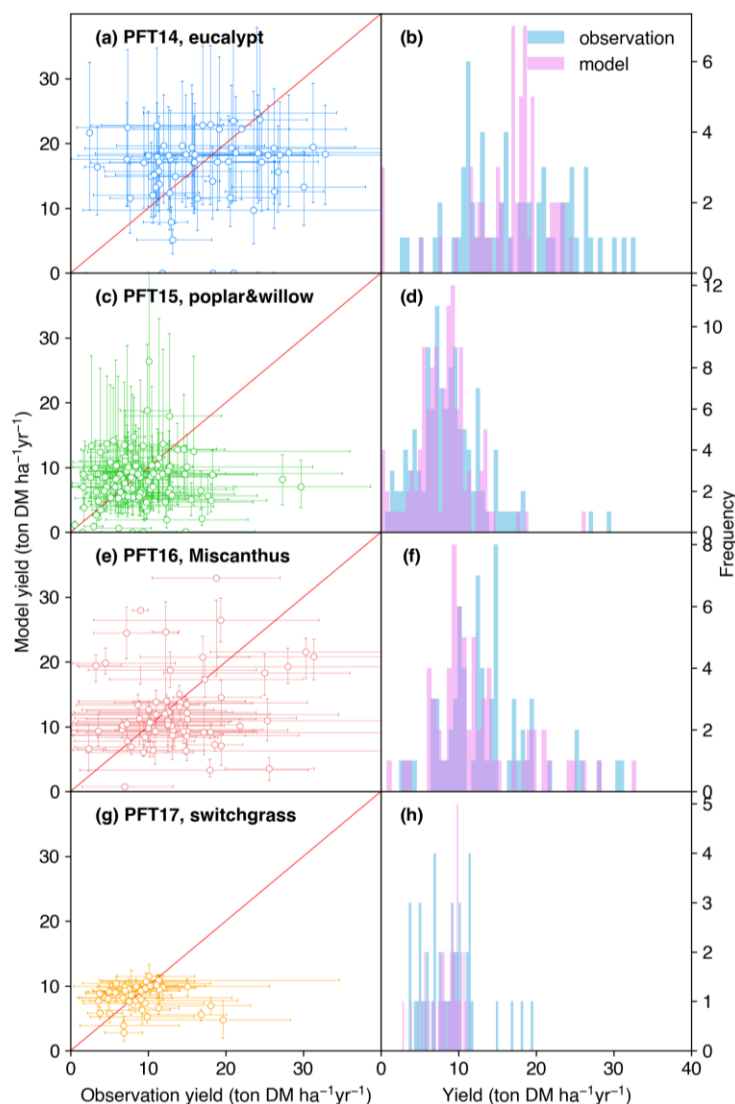
Figure 3 Biomass yields from the observations and simulated by the ORCHIDEE model. The error bars of observations in the left panel represent the range of different observations in this half degree grid cell caused by different sites, treatments, species and genotypes. The error bars of modelled yields represent the range of different harvest years caused by inter annual variability of climate. PFT 14 is tropical bioenergy tree, eucalypt; PFT15 is temperate bioenergy tree, poplar and willow; PFT16 is C4 bioenergy grass, *Miscanthus*; PFT17 is C4 bioenergy grass, switchgrass. The red line indicates the 1:1 ratio line.

Geoscientific
Model Development
Discussions
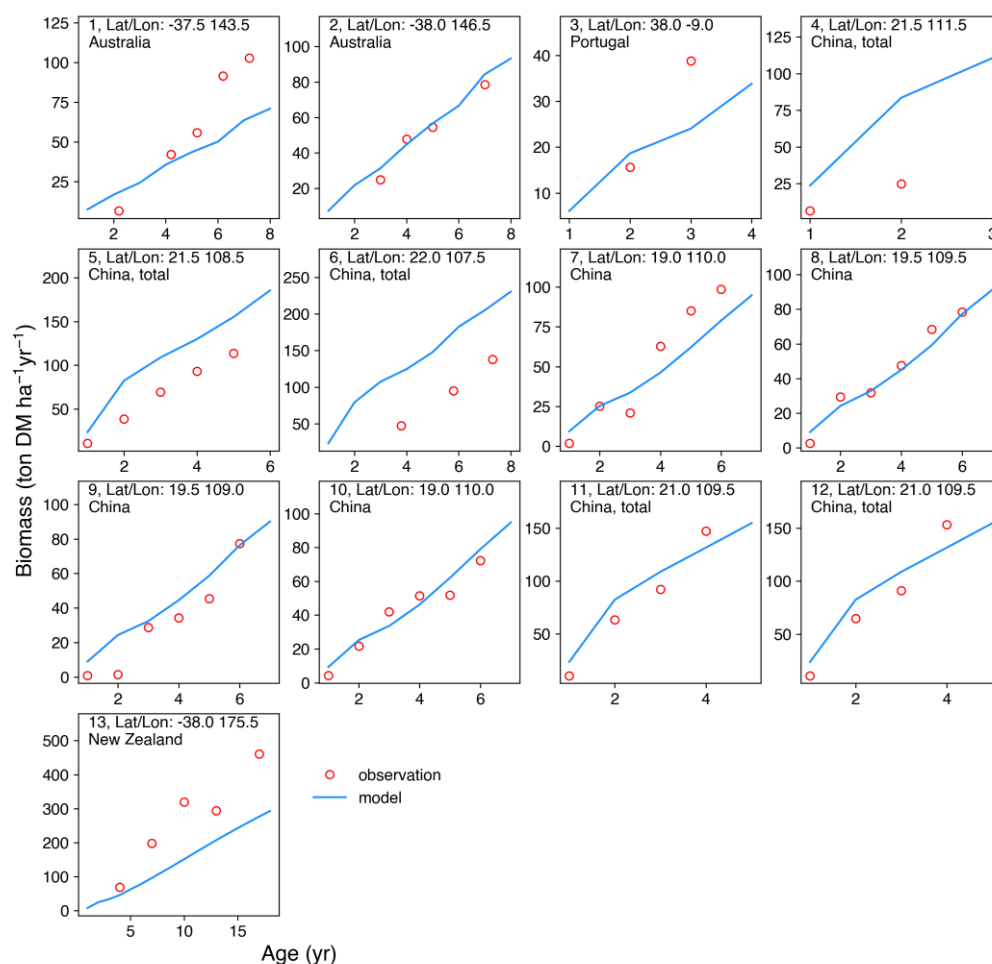
Figure 4 Biomass-age curves at different sites for PFT14 (tropical bioenergy tree, eucalypt). Site number, coordinates, and country for each site are also shown. Biomass at most sites refers to aboveground biomass, except Site #5, #11 and #12 (labeled "total", i.e. the sum aboveground and belowground biomass; the same total biomass from model is used for these sites). The detailed site information is shown in Table S2.
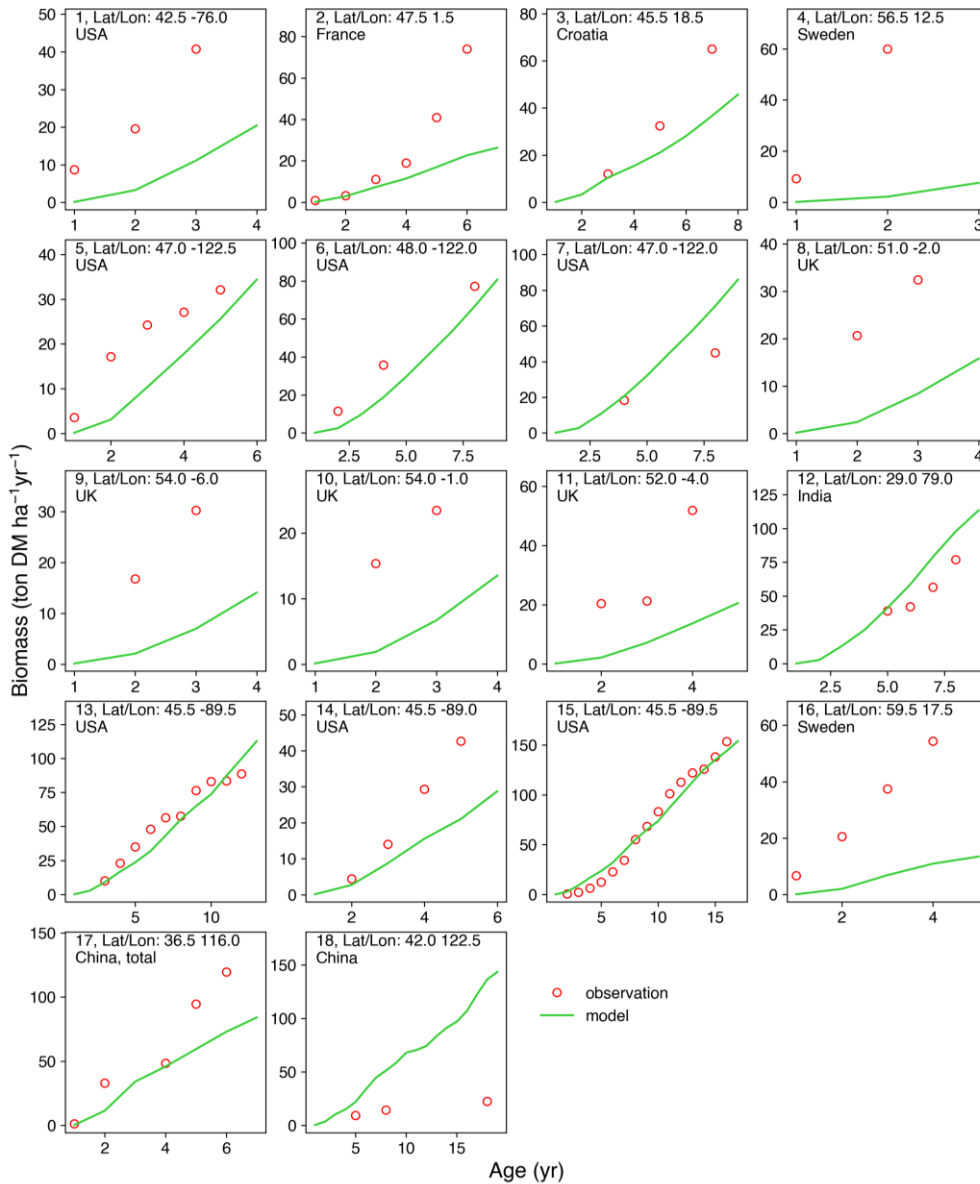
Figure 5 Biomass-age curves at different sites for PFT15 (temperate bioenergy tree, poplar and willow). Site number, coordinates, and country for each site are also shown. Biomass at most sites refers to aboveground biomass, except Site #17 (labeled "total", i.e. the sum aboveground and belowground biomass; the same total biomass from model is used for this site.). The detailed site information is shown in Table S2.
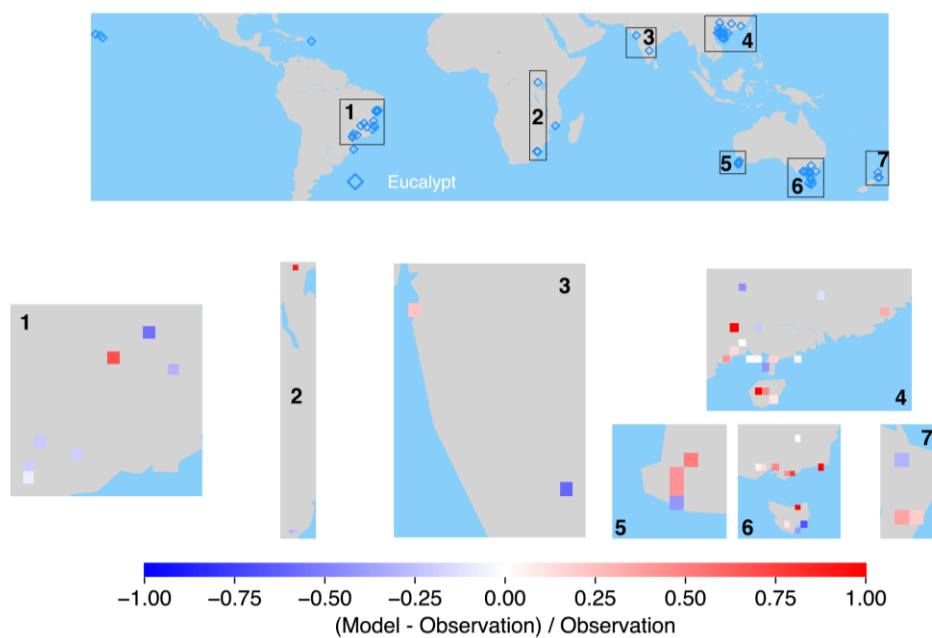
Figure 6 The map of relative difference between simulated and observed biomass yields for PFT14 (tropical bioenergy tree, eucalypt).
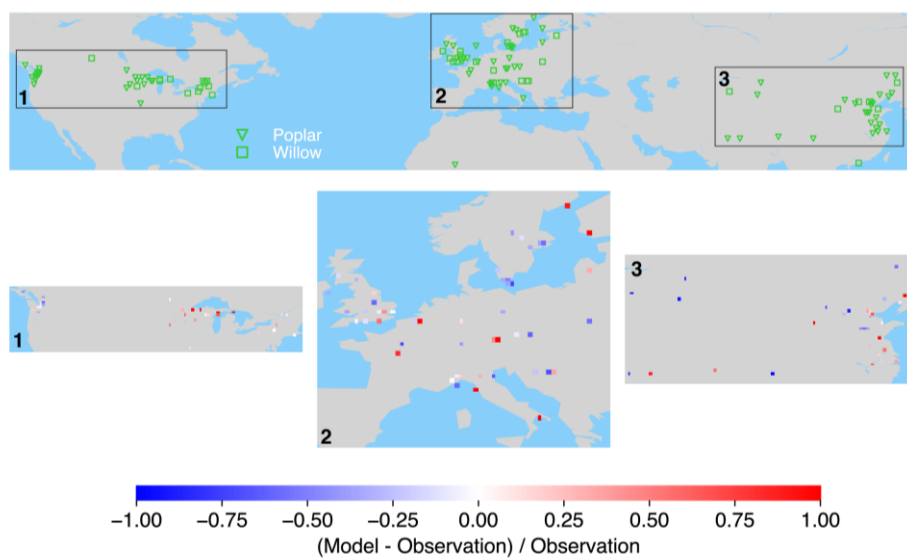
Figure 7 The map of relative difference between simulated and observed biomass yields for PFT15 (temperate bioenergy tree, poplar and willow).
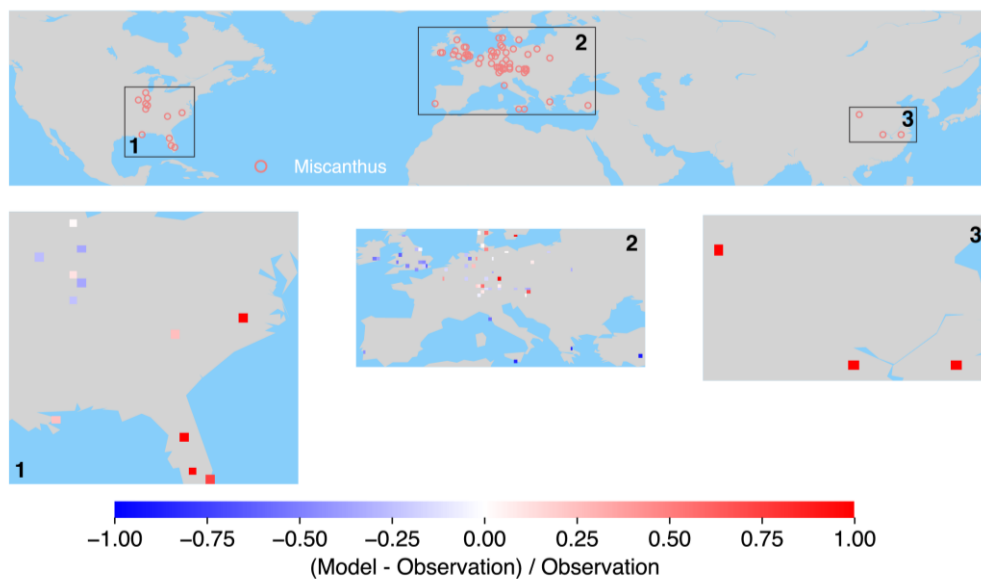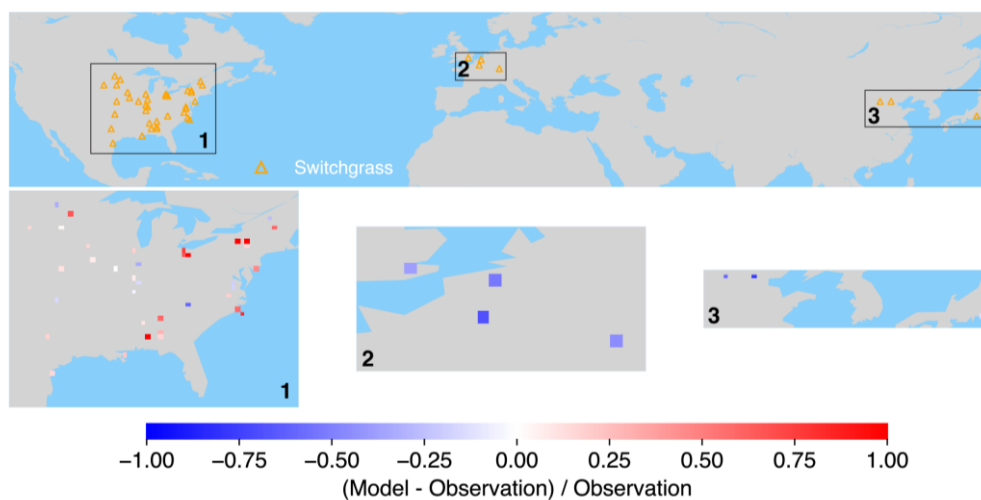
Figure 8 The map of relative difference between simulated and observed biomass yields for PFT16 (C4 bioenergy grass, *Miscanthus*).

Figure 9 The map of relative difference between simulated and observed biomass yields for PFT17 (C4 bioenergy grass, switchgrass).
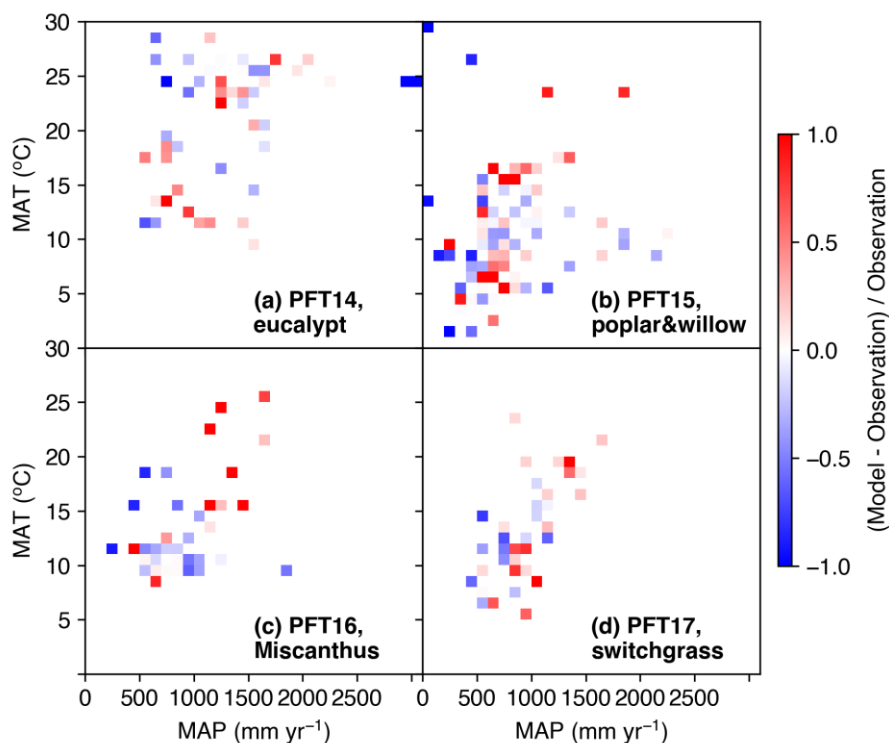
Figure 10 The relative difference between simulated and observed yield in different MAT and MAP intervals. The median values of model-observation differences of all grid cells in each MAT and MAP intervals are shown. PFT 14 is tropical bioenergy tree, eucalypt; PFT15 is temperate bioenergy tree, poplar and willow; PFT16 is C4 bioenergy grass, *Miscanthus*; PFT17 is C4 bioenergy grass, switchgrass. The red line indicates the 1:1 ratio line.
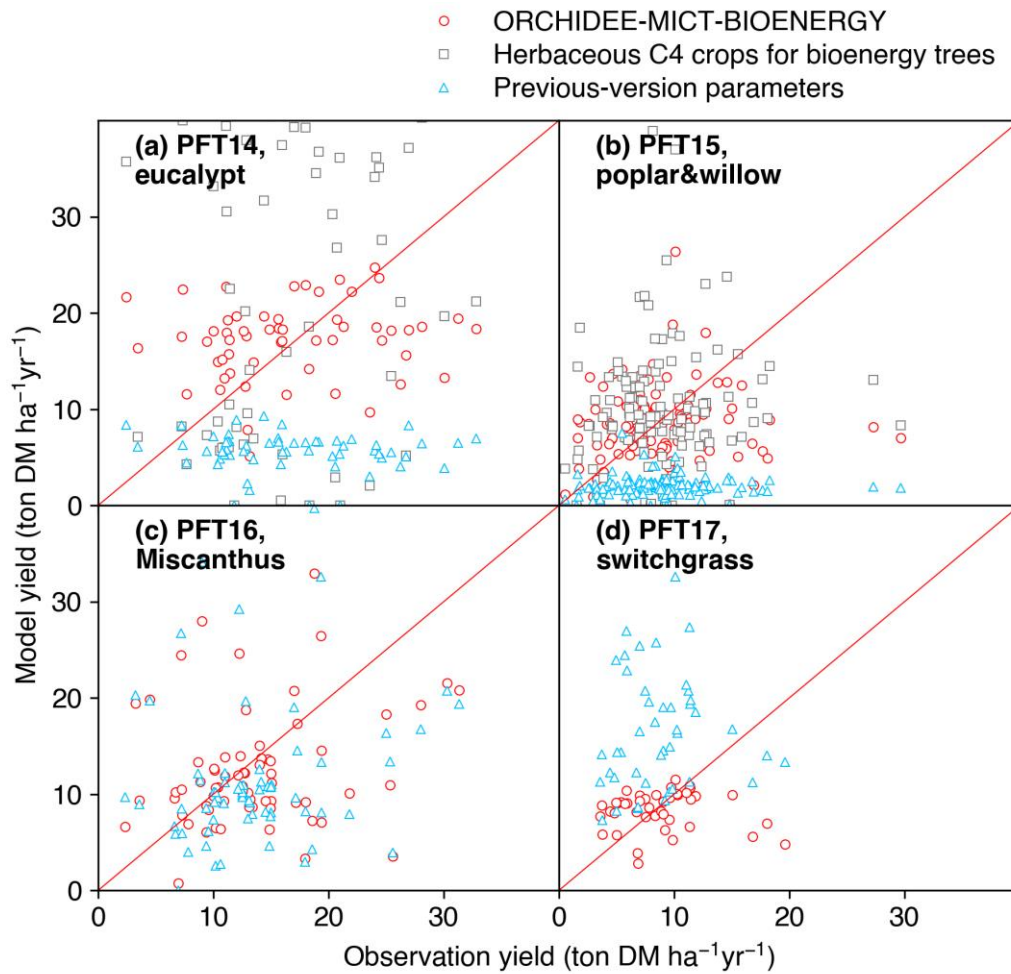
5

Figure 11 Comparison of biomass yields simulated by ORCHIDEE-MICT-BIOENERGY and previous versions. Only median values in half-degree grid cells, some containing multiple sites, are shown for both simulated and observed yields. Red circles represent the simulations using specific bioenergy parameterizations (same as Fig. 3). Grey squares represent using the herbaceous crop PFTs of previous ORCHIDEE version for bioenergy trees, i.e. PFT13 for both PFT14 and PFT15 (Table 2). Blue triangles represent the simulations using the right PFTs but the parameters of previous ORCHIDEE version, i.e. parameters of PFT2 (Tropical Broad-leaved Evergreen), PFT6 (Temperate Broad-leaved Summergreen), PFT13 (C4 Crop) and PFT13 (C4 Crop) for PFT14 (eucalypt), PFT15 (poplar and willow), PFT16 (*Miscanthus*) and PFT17 (switchgrass), respectively (Table 2).

Table 1. Plant functional types (PFTs) in ORCHIDEE. The newly added bioenergy PFTs (PFT14 to PFT17) use the default setting of the original PFTs (all processes except harvest, see Section 2.2) but with new parameterizations (see Section 2.3).

PFT No.	Name
1	Bare soil
2	Tropical Broad-leaved Evergreen
3	Tropical Broad-leaved Raingreen
4	Temperate Needleleaf Evergreen
5	Temperate Broad-leaved Evergreen
6	Temperate Broad-leaved Summergreen
7	Boreal Needleleaf Evergreen
8	Boreal Broad-leaved Summergreen
9	Boreal Needleleaf Summergreen
10	C3 Grass
11	C4 Grass
12	C3 Crop
13	C4 Crop
14 = 2	Tropical Bioenergy Tree, representing Eucalypts (*Eucalyptus spp.*)
15 = 6	Temperate Bioenergy Tree, representing poplar (*Populus spp.*) and willow (*Salix spp.*)
16 = 13	Bioenergy Grass *Miscanthus*
17 = 13	Bioenergy Grass Switchgrass (*Panicum spp.*)

5

Table 2. Parameters adjusted for bioenergy crop PFTs in ORCHIDEE-MICT. Values of original PFTs are also shown for comparison.

Symbol	Parameter	Definition	Unit	PFT2, Tropical Broad-leaved Evergreen — Value	PFT4, Tropical Bioenergy Tree, eucalypt — Value	PFT4 — Reference	PFT6, Temperate Broad-leaved Deciduous — Value	PFT15, Temperate Bioenergy Tree, poplar and willow — Value	PFT15 — Reference	PFT13, C4 crop — Value	PFT16, Bioenergy Grass_Miscanthus — Value	PFT16 — Reference	PFT17, Bioenergy Grass_Switchgrass — Value	PFT17 — Reference
Photosynthesis parameter														
V_{cmax25}	VCMAX25	Maximum rate of Rubisco activity-limited carboxylation at 25 ℃	$\mu mol\ CO_2\ m^{-2}\ s^{-1}$	65	100	this study	55	70	this study	70	25	this study	20	this study
a_{JV}	ARJV	Coefficient of the linear regression defining the J_{max}/V_{cmax} ratio	$\mu mol\ e^-\ (\mu mol\ CO_2)^{-1}$	2.59	2.63	this study	2.59	2.99	this study	1.715	3.5	this study	2	this study
b_{JV}	BRJV	Coefficient of the linear regression defining the J_{max}/V_{cmax} ratio	$\mu mol\ e^-\ (\mu mol\ CO_2)^{-1}\ {}^\circ C^{-1}$	-0.035	-0.035	default	-0.035	-0.035	default	0	0	default	0	default
θ	THETA	Convexity factor for response of rate of e⁻ transport to irradiance	-	0.7	0.8	Yin and Struik, 2017	0.7	0.7	default	0.7	0.84	Dohleman and Long, 2009	0.7	default
$\alpha_{(LL)}$	ALPHA_LL	Conversion efficiency of absorbed light into e⁻ transport rate at strictly limiting light	$mol\ e^-\ (mol\ photo)^{-1}$	0.3	0.43	Yin and Struik, 2009	0.3	0.43	Yin and Struik, 2009	0.3	0.43	Yin and Struik, 2009	0.43	Yin and Struik, 2009
g_0	G0	Residual stomatal conductance when irradiance approaches zero	$mol\ CO_2\ m^{-2}\ s^{-1}\ bar^{-1}$	0.00625	0.01875	this study	0.00625	0.01875	this study	0.01875	0.01875	default	0.01875	default
SLA / SLA_MAX / SLA_MIN	SLA	Specific leaf area	$m^2\ g^{-1}\ C$	0.0153	0.02	this study	0.026	0.04	this study	0.026	0.029	this study	0.04	this study
k	EXT_COEFF	Light extinction coefficient	-	0.5	0.36	Stape et al., 2004	0.5	0.3	Heilman et al., 1996	0.5	0.5	default	0.5	default
LAI_{max}	LAI_MAX	maximum leaf area index, beyond which no carbon is allocated to leaf	-	7	7	Whitehead and Beadle, 2004	5	9	Ceulemans et al., 1992; Heilman et al., 1996	5	10	Heaton et al., 2008; Zub and Brancourt-Hulmel, 2010	8	Heaton et al., 2008
Carbon allocation parameter														
τ	DEMI_ALLOC	A constant in the function to calculate aboveground sapwood allocation for tree PFTs	year	5	2	this study	5	2	this study	-	-	-	-	-
β	HYDROL_HUMCSTE	The factor in the exponential function to calculate the soil water stress	-	0.8	0.6	this study	0.8	0.6	this study	4	4	default	4	default
Phenology parameter														
GDD_{onset}	PHENO_GDD_CRIT_C	The growing degree days to determine leaf onset	degree-day	-	-	-	-	-	-	700	320	set to the default value of C4 grass (PFT11); Zub and Brancourt-Hulmel, 2010	320	set to the default value of C4 grass (PFT11) ; Zub and Brancourt-Hulmel, 2010
$T_{senescence}$	SENESCENCE_TEMP_C	The critical temperature for leaf senescence	℃	-	-	-	12	12	default	10	0	Zub and Brancourt-Hulmel, 2010	0	Zub and Brancourt-Hulmel, 2010
t_{leaf}	LEAFAGECRIT	Critical leaf age, beyond which leaves fall off	day	730	730	default	180	180	default	90	120	set to the default value of C4 grass (PFT11)	120	set to the default value of C4 grass (PFT11)
$t_{leaf,min}$	MIN_LEAF_AGE_FOR_SENESCENCE	Minimum leaf age to allow leaf senescence	day	-	-	-	90	90	default	30	90	set to the default value of C4 grass (PFT11)	90	set to the default value of C4 grass (PFT11)
Harvest parameter														
HI	FRAC_BIOENERGY_HARVEST	Harvest index, fraction of aboveground biomass that is harvested	-	-	0.9	Richards et al., 2017; Zhuang et al., 2013	-	0.9	Richards et al., 2017; Zhuang et al., 2013	-	0.9	Caslin et al., 2010; Richards et al., 2017	0.9	Richards et al., 2017
R	ROTATION_LENGTH	The rotation length of short-rotation trees; this parameter is determined by the setting-up of forest age classes	year	-	4–6	this study	-	4–6	this study	-	-	-	-	-